

## Article

# Cu-IM-5 as the Catalyst for Selective Catalytic Reduction of NO<sub>x</sub> with NH<sub>3</sub>: Role of Cu Species and Reaction Mechanism

Guangying Fu <sup>1</sup>, Junwen Chen <sup>2</sup>, Yuqian Liang <sup>1</sup>, Rui Li <sup>1</sup>, Xiaobo Yang <sup>3,\*</sup> and Jiuxing Jiang <sup>1,\*</sup> 

<sup>1</sup> MOE Key Laboratory of Bioinorganic and Synthetic Chemistry, School of Chemistry, Sun Yat-sen University, Guangzhou 510275, China; fugy5@mail2.sysu.edu.cn (G.F.); liangyq38@mail2.sysu.edu.cn (Y.L.); lirui99@mail2.sysu.edu.cn (R.L.)

<sup>2</sup> State Key Laboratory of Catalytic Materials and Reaction Engineering, Research Institute of Petroleum Processing, SINOPEC, Beijing 100083, China; chenjw.ripp@sinopec.com

<sup>3</sup> The ZeoMat Group, Qingdao Institute of Bioenergy and Bioprocess Technology, Chinese Academy of Sciences, Qingdao 266101, China

\* Correspondence: yangxb@qibebt.ac.cn (X.Y.); jiangjiux@mail.sysu.edu.cn (J.J.); Tel.: +86-20-84111355 (J.J.)

**Abstract:** The role of Cu species in Cu ion-exchanged IM-5 zeolite (Cu-IM-5) regarding the performance in selective catalytic reduction (SCR) of NO<sub>x</sub> with NH<sub>3</sub> (NH<sub>3</sub>-SCR) and the reaction mechanism was studied. Based on H<sub>2</sub> temperature-programmed reduction (H<sub>2</sub>-TPR) and electron paramagnetic resonance (EPR) results, Cu–O–Cu and isolated Cu species are suggested as main Cu species existing in Cu-IM-5 and are active for SCR reaction. Cu–O–Cu species show a good NH<sub>3</sub>-SCR activity at temperatures below 250 °C, whereas their NH<sub>3</sub> oxidation activity at higher temperatures hinders the SCR performance. At low temperatures, NH<sub>4</sub>NO<sub>3</sub> and NH<sub>4</sub>NO<sub>2</sub> are key reaction intermediates. In situ diffuse reflectance infrared Fourier transform spectroscopy (DRIFTS) suggests a mixed Eley–Rideal (E–R) and Langmuir–Hinshelwood (L–H) mechanism over Cu-IM-5 at low temperatures.



**Citation:** Fu, G.; Chen, J.; Liang, Y.; Li, R.; Yang, X.; Jiang, J. Cu-IM-5 as the Catalyst for Selective Catalytic Reduction of NO<sub>x</sub> with NH<sub>3</sub>: Role of Cu Species and Reaction Mechanism. *Catalysts* **2021**, *11*, 221. <https://doi.org/10.3390/catal11020221>

Academic Editor: Franck Launay  
Received: 20 January 2021  
Accepted: 4 February 2021  
Published: 7 February 2021

**Publisher's Note:** MDPI stays neutral with regard to jurisdictional claims in published maps and institutional affiliations.



**Copyright:** © 2021 by the authors. Licensee MDPI, Basel, Switzerland. This article is an open access article distributed under the terms and conditions of the Creative Commons Attribution (CC BY) license (<https://creativecommons.org/licenses/by/4.0/>).

**Keywords:** NH<sub>3</sub>-SCR; Cu-IM-5; in situ DRIFTS; reaction mechanism

## 1. Introduction

Selective catalytic reduction (SCR) of nitrogen oxides (NO<sub>x</sub>) with NH<sub>3</sub> is an effective way of eliminating environmentally harmful NO<sub>x</sub> in the exhaust gases from vehicles, ships, and electric plants. The biggest challenge of the research is to eliminate NO<sub>x</sub> from the oxygen-rich exhaust gas of diesel engines and to design practical diesel SCR catalysts [1]. Transition metal ion-exchanged zeolites (Cu, Fe, etc.) have been extensively studied and applied as commercial SCR catalysts in diesel-powered vehicles due to the excellent performance, i.e., high activity, high N<sub>2</sub> selectivity, and hydrothermal stability [2].

Many zeolites with various framework types, such as MFI, BEA, CHA, AEI, ERI, KFI, AFX, DDR, RTH, SFW, LEV, LTA, RHO, and UFI, have been investigated as SCR catalysts [3–8]. Iwamoto et al. [9,10] first reported the catalytic activity of Cu-ZSM-5 for the decomposition of NO. Later, the catalyst became one of the most investigated zeolite materials for SCR. ZSM-5 (MFI topology) consists of an intersected 2D channel system, i.e., the straight channel along the *b*-axis and the sinusoidal channel along the *a*-axis. Both channels are delimited by 10-rings of TO<sub>4</sub> (Si, Al) tetrahedral with pore openings 5.1 × 5.5 Å in size. Zeolite IM-5 (IMF topology) shows a similar 10-ring pore opening with ZSM-5, but a different 3D intersected channel system. IM-5 consists of two straight channels along the *a*-axis/*c*-axis, and a tortuous channel along the *b*-axis [11]. The zeolite is an excellent alternative to ZSM-5 in various reactions [12,13], especially for the NH<sub>3</sub>-SCR reaction. Vennestrøm et al. [14] found that IM-5 shows higher framework Al stability than ZSM-5 against hydrothermal treatments. However, the role of Cu species in SCR and the reaction mechanism were not fully understood yet.

In addition to the zeolite framework, Cu species are also studied intensively. As commonly accepted, isolated  $\text{Cu}^{2+}$  ions are the best catalytic active sites;  $\text{CuAl}_2\text{O}_4$  species are inactive in the reaction; other species such as  $[\text{Cu}(\text{OH})]^+-\text{Z}$  and  $[\text{Cu}-\text{O}-\text{Cu}]^{2+}$  are still in debate [2,15–18]. Gao et al. [19] observed  $\text{NH}_3$  oxidation followed  $[\text{Cu}-\text{O}-\text{Cu}]^{2+}$  species formation under high levels of Cu ion-exchange degree. Recently, Liu et al. [20] demonstrated that highly dispersed  $\text{CuO}_x$  (such as  $\text{Cu}-\text{O}-\text{Cu}$ ) can also catalyze  $\text{NO}_x$  reduction at a high temperature, i.e., 425 °C.  $[\text{Cu}(\text{OH})]^+-\text{Z}$  sites are more effective for  $\text{NO}_x$  reduction at low temperatures but more selective for  $\text{NH}_3$  oxidation at high temperatures. Szanyi et al. [21,22] found that nitrosyl species bounded to copper are key intermediates during  $\text{NH}_3$ -SCR. NO is firstly oxidized to  $\text{NO}_2$ , then  $\text{NO}_2$  transforms to surface nitrates and nitrosyl species [23,24].

The purpose of this study is to illuminate Cu species in Cu-IM-5 and to illustrate the reaction mechanism toward  $\text{NH}_3$ -SCR. In this study, Cu-IM-5 with different Cu contents were prepared through the ion-exchange method. The  $\text{NH}_3$ -SCR performance was tested. Then, a combination of several characterization techniques is applied and correlated with the catalytic performance in  $\text{NH}_3$ -SCR reaction, i.e., inductively coupled  $\text{H}_2$  temperature-programmed reduction ( $\text{H}_2$ -TPR),  $\text{NH}_3$ -temperature-programmed desorption ( $\text{NH}_3$ -TPD), electron paramagnetic resonance (EPR), UV-vis-NIR, XPS, and in situ DRIFTS. In addition, the mechanism of SCR is investigated through in situ DRIFTS.

## 2. Results

### 2.1. Structure Characterization

A sample of zeolite IM-5 was chosen as the parent material, and a number of Cu-IM-5 catalysts with various Cu-loading amounts were prepared via ion-exchange in diluted  $\text{Cu}(\text{NO}_3)_2$  solutions. Table 1 lists the elemental analysis of IM-5 and Cu-IM-5, and some other relevant characteristics. According to inductively coupled plasma atomic emission spectroscopy (ICP-AES) analysis, Si/Al ratios of IM-5 and ion-exchanged Cu-IM-5 samples remain practically unchanged (between 16.5 and 17.2). Cu contents of the ion-exchanged samples are 1.4 wt.%, 1.8 wt.%, and 2.3 wt.%, respectively, corresponding Cu exchange-rates are 0.56, 0.80, and 0.90. These samples are denoted according to their Cu contents, i.e., 1.4Cu-IM-5, 1.8Cu-IM-5, and 2.3Cu-IM-5, respectively.

**Table 1.** Element analysis and physical properties of the relevant samples.

Sample	Si/Al (ICP)	Framework Si/Al <sup>1</sup>	Cu Contents wt.%	Cu/2Al	EPR Signal Intensity ( $g_{\perp}$ )	$S_{\text{BET}}$ m <sup>2</sup> /g	Pore Volume cm <sup>3</sup> /g
IM-5	16.5	13.9	0	0	0	354.9	0.375
1.4Cu-IM-5	16.8	12.8	1.4	0.56	$6.4 \times 10^6$	347.7	0.370
1.8Cu-IM-5	17.2	12.5	1.8	0.80	$3.2 \times 10^6$	336.3	0.358
2.3Cu-IM-5	16.7	12.3	2.3	0.90	$2.1 \times 10^6$	328.9	0.345

<sup>1</sup> Calculated by <sup>29</sup>Si MAS NMR.

Powder X-ray diffraction (PXRD) (Figure 1a) of IM-5 and Cu-IM-5 with different Cu contents show characteristic diffraction peaks of IMF topology, which are well fitted with the simulated pattern, suggesting the stability of the IM-5 framework under ion exchange conditions. Peaks that are characteristic of CuO ( $2\theta = 35.6$  and  $38.8^\circ$ ) are absent in all Cu-IM-5 samples, implying that CuO crystals are not present even at higher ion-exchange rates.  $\text{N}_2$  adsorption-desorption isotherms of IM-5 and Cu-IM-5 samples (Figure 1b) are typical for the typical type I, which is characteristic of microporous materials. Calculated BET specific surface areas and pore volumes are listed in Table 1. IM-5 has a pore volume of 0.375 cm<sup>3</sup>/g with a BET surface area of 354.9 m<sup>2</sup>/g. After ion-exchanges with Cu, BET surface areas and pore volumes have decreased slightly with increasing Cu contents. As shown in Figure 1c,d, IM-5 consists of large particles, which are stacks of rod-like nanocrystals with lengths of ca. 300 nm. The morphology of 1.4Cu-IM-5, as an example

for the ion-exchanged catalysts, is identical to the parent IM-5. The ion-exchange affects neither the crystal structure nor the morphology, as expected normally for zeolite materials.

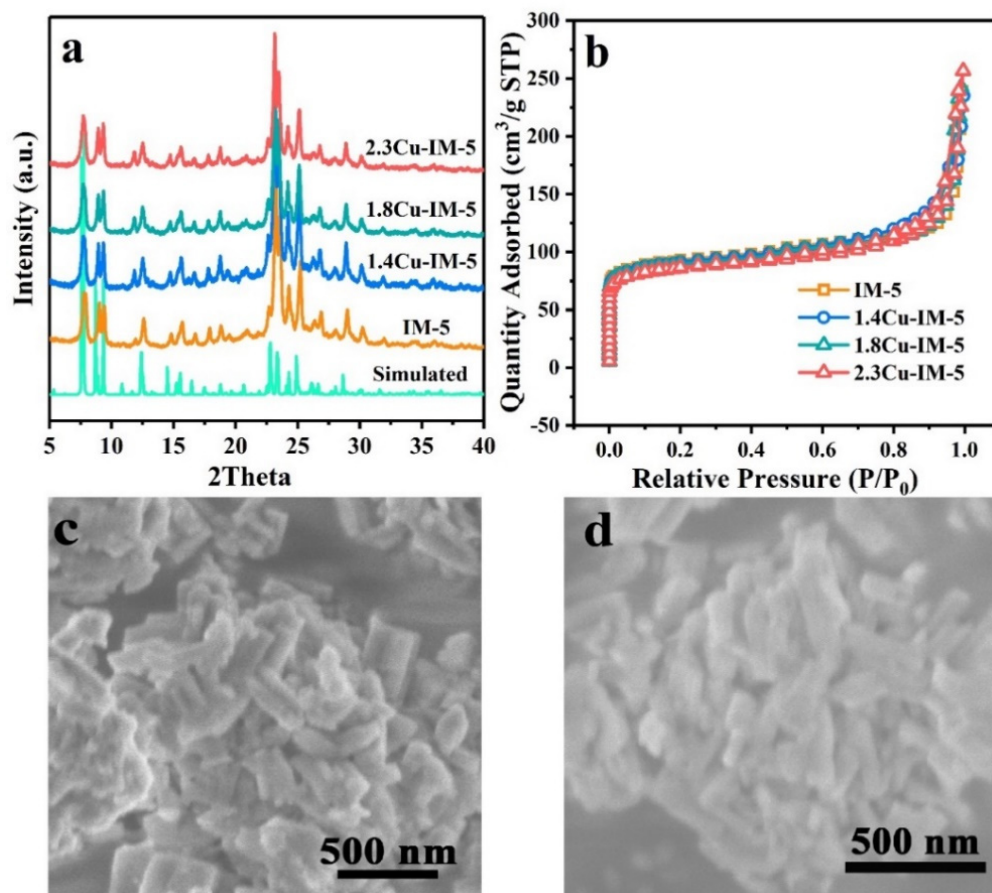


**Figure 1.** (a) Powder X-ray diffraction (PXRD) patterns, (b)  $N_2$  adsorption and desorption curves, (c) SEM images of IM-5, and (d) 1.4Cu-IM-5.

As shown in Figure 2, the scanning transmission electron microscopy (STEM) image of 2.5Cu-IM-5 shows the typical morphology of IM-5, which is identical to that in Figure 1. The high dispersion of Cu species was further checked by EDS mapping.

$^{29}\text{Si}$  and  $^{27}\text{Al}$  MAS NMR spectra of IM-5 and Cu-IM-5 samples are illustrated in Figure 2. As shown in Figure 3a,  $^{29}\text{Si}$  resonances at  $-98$ ,  $-101$ ,  $-106$ , and  $-112$  ppm are assigned to  $Q^4(3)$ ,  $Q^4(2)$ ,  $Q^4(1)$ , and  $Q^4(0)$ . Calculated Si/Al ratios by  $^{29}\text{Si}$  MAS NMR and ICP (Table 1) are in good agreement for IM-5 and Cu-IM-5 samples. In  $^{27}\text{Al}$  MAS NMR spectra (Figure 3b) of IM-5 and Cu-IM-5, only tetrahedral-coordinated Al are detected at  $\delta = 58$  ppm.

## 2.2. $\text{NH}_3$ -SCR Performance over Cu-IM-5

Figure 4a shows the  $\text{NO}_x$  conversions during  $\text{NH}_3$ -SCR with IM-5 and Cu-IM-5 samples. IM-5 shows almost no activity for  $\text{NO}_x$  reduction at low temperatures. For 1.4Cu-IM-5,  $\text{NO}_x$  conversion shows a volcano-shaped line with increasing temperature. The maximum  $\text{NO}_x$  conversion reaches 96.6% at 250 °C, then declines due to  $\text{NH}_3$  oxidation [14]. With increasing Cu contents, the  $\text{NO}_x$  conversion increases slightly at low temperatures between 150 °C and 250 °C. However, in the high-temperature region (300–550 °C),  $\text{NO}_x$  conversion declines with increasing Cu contents, which can be attributed to an increasing  $\text{NH}_3$  oxidation activity. It is worth noting that 1.4Cu-IM-5 exhibits higher  $\text{NO}_x$  conversion than Cu-IM-5 from 200 °C to 550 °C. As shown in Figure 4b, high  $\text{N}_2$  selectivity was achieved overall Cu-IM-5 catalysts.  $\text{N}_2$  selectivity of 1.4Cu-IM-5 was 84.8% at 150 °C and then

increases to 98% at 250 °C and starts to decline at 350 °C. The same trend of N<sub>2</sub> selectivity against temperatures was found for 1.8Cu-IM-5 and 2.3Cu-IM-5 as well. Figure 4c shows NH<sub>3</sub> oxidation on Cu-IM-5 from 250 °C to 550 °C. For NH<sub>3</sub>-SCR, NH<sub>3</sub> oxidation is the primary side reaction, and NO is the main side product at high temperatures [25]. With increasing Cu contents, NH<sub>3</sub> conversion rises, and NO<sub>x</sub> concentration increases. At high temperatures (>300 °C), there is insufficient NH<sub>3</sub> to reduce NO, and NO is produced from NH<sub>3</sub> oxidation. Hence, the apparent NO<sub>x</sub> conversion decreases at high temperatures. The slightly decreasing N<sub>2</sub> selectivity with increasing Cu contents is also a consequence of the increasing NH<sub>3</sub> oxidation.

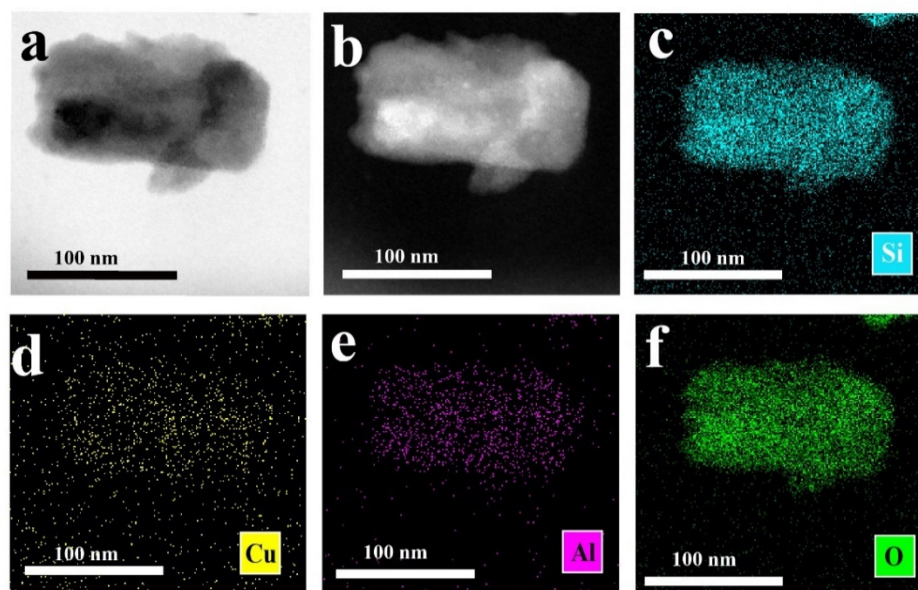


Figure 2. STEM images (a,b; scale bar corresponds 50 nm); and EDS mapping (b–f; scale bar corresponds 100 nm) of 2.3Cu-IM-5.

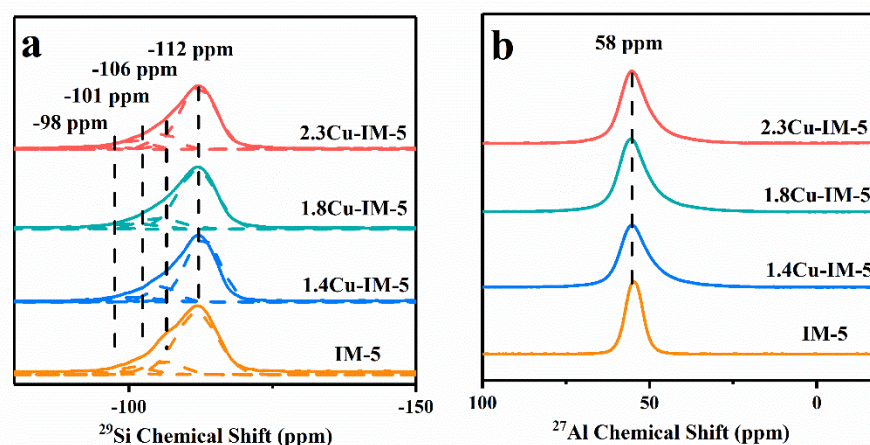


Figure 3. (a) Si and (b) <sup>27</sup>Al MAS NMR spectra of Cu-IM-5 with different Cu loadings.

### 2.3. Cu Species in Cu-IM-5

In order to evaluate the oxidation states of Cu species on the outer surfaces of Cu-IM-5, XPS analysis of Cu 2p core level was performed (Figure 5a). Peaks located at the binding energies of  $933.8 \pm 0.2$  eV and  $953.9 \pm 0.2$  eV are ascribed to Cu 2p<sub>3/2</sub> and Cu 2p<sub>1/2</sub>, respectively. Shakeup peaks locate at 943 eV are essential characteristics of divalent Cu species [26]. Only one kind of peak at 933.8 eV assigned to Cu<sup>2+</sup> species is observed,

suggesting that all divalent copper species existing in Cu-IM-5 are similar. The intensity of this peak rises with increasing Cu contents.

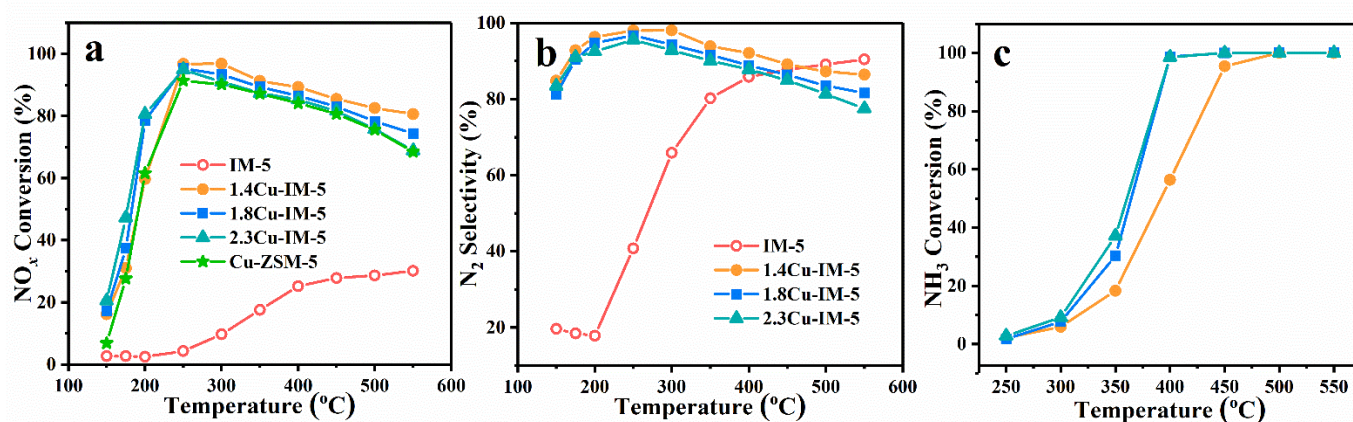


Figure 4. (a)  $\text{NO}_x$  conversion, (b)  $\text{N}_2$  selectivity, and (c)  $\text{NH}_3$  oxidation over IM-5 and Cu-IM-5 with different Cu contents.

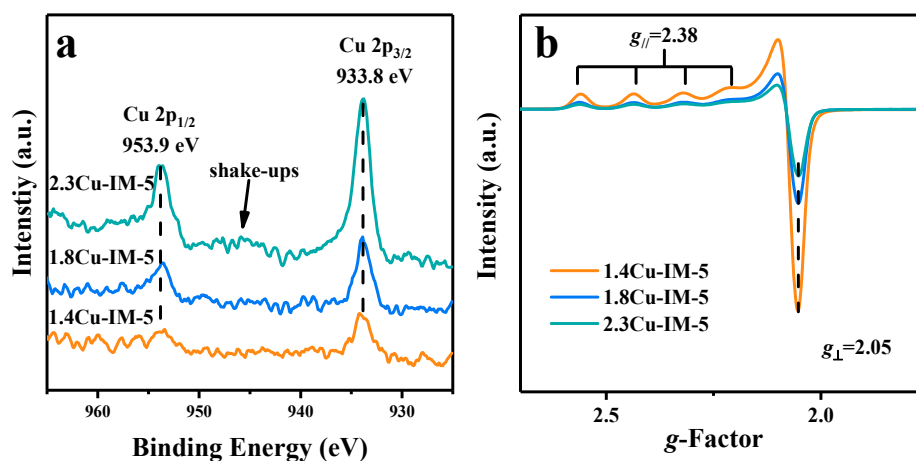
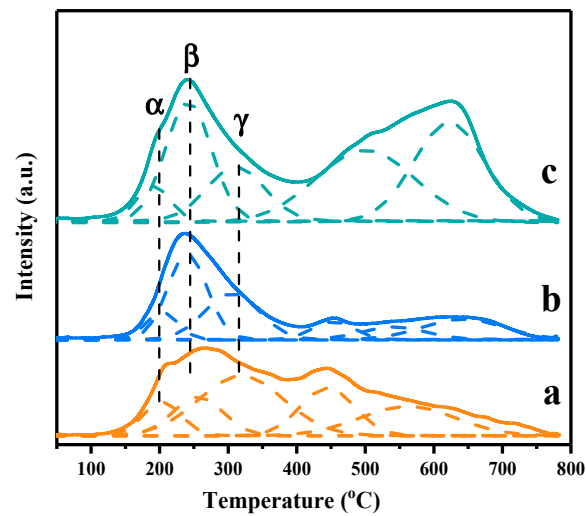


Figure 5. (a) XPS (b) and electron paramagnetic resonance (EPR) of Cu-IM-5 with different Cu loadings.

EPR spectra reveal the number of isolated Cu ions (Figure 5b). Therefore, only isolated  $\text{Cu}^{2+}$  species can be detected, while other species such as  $\text{Cu}^+$  and  $\text{CuO}_x$  clusters are inactive [27]. All samples show  $g_{\perp} = 2.05$  and  $g_{\parallel} = 2.38$ , which are typical of isolated hydrated  $\text{Cu}^{2+}$  complexes in a distorted octahedral symmetry such as  $[\text{Cu}(\text{H}_2\text{O})_6]^{2+}$  and  $[\text{Cu}(\text{H}_2\text{O})_5(\text{OH})]^+$  [28]. The intensity of  $g_{\perp}$  peak at high frequency decreases from  $6.4 \times 10^6$  to  $2.1 \times 10^6$  with increasing Cu contents. The decreasing intensity of  $g_{\perp}$  peak results from the loss of isolated  $\text{Cu}^{2+}$  ions, which aggregate and form  $\text{Cu}-\text{O}-\text{Cu}$  [28].

$\text{H}_2$ -TPR is to study the reducibility of Cu-IM-5 with various Cu contents. As shown in Figure 6, the curves are fitted to quantify different Cu species, and the results are shown in Table 2. Three kinds of peaks are clearly shown during 150–400 °C: the peaks centered at about 200 °C is attributed to the reduction of isolated  $[\text{Cu}(\text{OH})]^+$  to  $\text{Cu}^+$ ; the peaks centered at about 240 °C is assigned to the reduction of divalent Cu in  $\text{Cu}-\text{O}-\text{Cu}$  type species to  $\text{Cu}^+$ ; the peak at 270 °C is assigned to the reduction of isolated  $\text{Cu}^{2+}$  species to  $\text{Cu}^+$ ; the peaks above 400 °C are assigned to the reduction of  $\text{Cu}^+$  to  $\text{Cu}^0$  [29,30]. For 1.4Cu-IM-5, the peak at 200 °C and 270 °C are observable, suggesting the presence of  $[\text{Cu}(\text{OH})]^+$  and  $\text{Cu}^{2+}$  species. With Cu contents reach to 1.8 wt.%, a peak centered at 240 °C emerges, suggesting a formation of  $\text{Cu}-\text{O}-\text{Cu}$  species. The fraction of this peak increases when Cu contents further increase.



**Figure 6.** Temperature-programmed reduction (TPR) curve of Cu-IM-5 with different Cu loadings: (a) 1.4Cu-IM-5, (b) 1.8Cu-IM-5, and (c) 2.3Cu-IM-5.

The acidity of Cu-IM-5 with different Cu contents is investigated using  $\text{NH}_3$ -TPD (Figure 7). To quantify the amount of the  $\text{NH}_3$  desorbed from different acid sites, the desorption curves have been fitted, and the fraction of the peaks are shown in Table 3. Two peaks shown in the curve of IM-5—the low-temperature peak (peak  $\alpha$ ) centered at 200 °C is ascribed to desorption of  $\text{NH}_3$  from weak acid (WA) sites, and the high-temperature peak (peak  $\gamma$ ) centered at 400 °C corresponds to the desorption of  $\text{NH}_3$  from strong acid (SA) sites. Cu-IM-5 samples exhibit a third peak (peak  $\beta$ ) at 300 °C, which is attributed to the desorption of  $\text{NH}_3$  from Cu ions [31]. At the same time, the peak center of  $\gamma$  moves to low temperatures (374 °C), indicating that strong acid sites of the aluminosilicate framework become weaker due to sheltering effects of extra-framework Cu ions. The fraction of peak  $\beta$  increases with increasing Cu loadings.

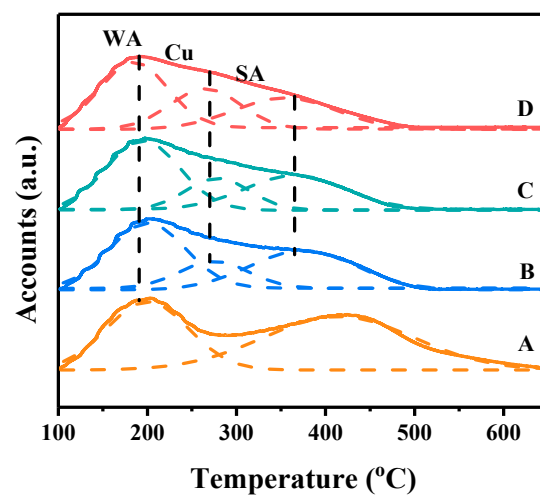


**Figure 7.**  $\text{NH}_3$ -temperature programmed desorption ( $\text{NH}_3$ -TPD) of Cu-IM-5 with different Cu loadings: (A) IM-5, (B) 1.4Cu-IM-5, (C) 1.8Cu-IM-5, and (D) 2.3Cu-IM-5.

**Table 2.** H<sub>2</sub>-TPR peak fractions of different Cu species.

Samples	[Cu(OH)] <sup>+</sup>	Cu–O–Cu	Cu <sup>2+</sup>
1.4Cu-IM-5	15.2	23.7	61.1
1.8Cu-IM-5	13.0	49.7	37.3
2.3Cu-IM-5	12.1	56.1	31.8

**Table 3.** Fractions of different desorption peaks in NH<sub>3</sub>-TPD curve.

Sample	Fraction of Different Peaks		
	Weak Acid	Cu Species	Strong Acid
IM-5	0.407	-	0.593
1.4Cu-IM-5	0.446	0.172	0.381
1.8Cu-IM-5	0.483	0.192	0.324

#### 2.4. Reaction Mechanisms

Taking 1.4Cu-IM-5 as an example, the catalyst is exposed to NO<sub>2</sub>, mixed with NO + O<sub>2</sub> (Figure 8), and observed using DRIFTS. The bands in the range of 1650 cm<sup>-1</sup> to 1500 cm<sup>-1</sup> are attributed to nitrate or nitro species adsorbed on Cu sites [29,32]. Bands at 1624 cm<sup>-1</sup>, 1613 cm<sup>-1</sup> (1597 cm<sup>-1</sup>), and 1573 cm<sup>-1</sup> (1545 cm<sup>-1</sup>) are ascribed to adsorbed NO<sub>2</sub> species, monodentate nitrates, bidentate nitrates, and nitrite adspecies [32,33], respectively. In NO<sub>2</sub>, the bands visibly increase with prolonging exposure time. Physically adsorbed NO<sub>2</sub> is swept off through N<sub>2</sub> for 30 min. Corresponding peaks decrease slightly. Exposed to mixed NO + O<sub>2</sub>, similar bands appear with lower intensity of IR bands. Wang et al. [32] reported that NO was first oxidized to NO<sub>2</sub> on Cu-SAPO-34. It is widely recognized that NO oxidation is the key factor for the further formation of nitrate and nitrite species [34]. Compared to the IR bands in NO<sub>2</sub> and NO + O<sub>2</sub> flow, the relative intensity of the NO<sub>2</sub> vibration band in the latter is stronger than that of the former, as a consequence that the existence of NO<sub>2</sub> suppresses the oxidation of NO.

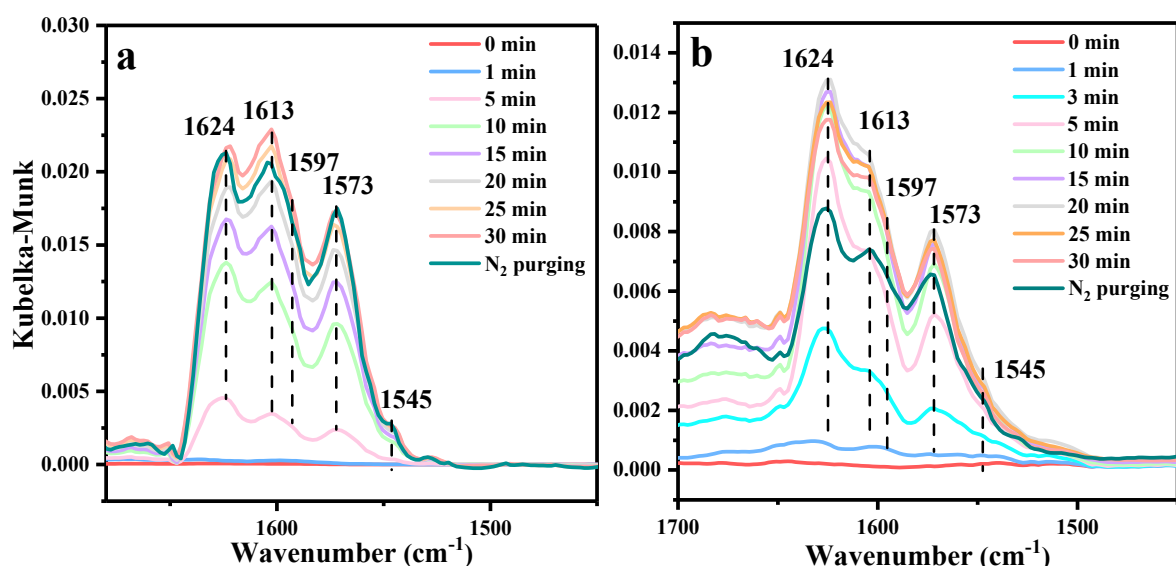


**Figure 8.** In situ DRIFTS of 1.4Cu-IM-5 exposed in (a) 500 ppm NO<sub>2</sub> and (b) 500 ppm NO + 5% O<sub>2</sub> followed by purging in N<sub>2</sub> for 30 min at 100 °C.

As shown in Figure 9, similar nitrate species are observed for Cu-IM-5 with different Cu contents after the exposure in NO + O<sub>2</sub> flow. The intensity of the IR bands, especially the bands of NO<sub>2</sub>, increases with increasing Cu contents. It indicates that NO is easier

oxidized on Cu-IM-5 with higher Cu content. Consequently, a higher amount of nitrates becomes observed by IR.

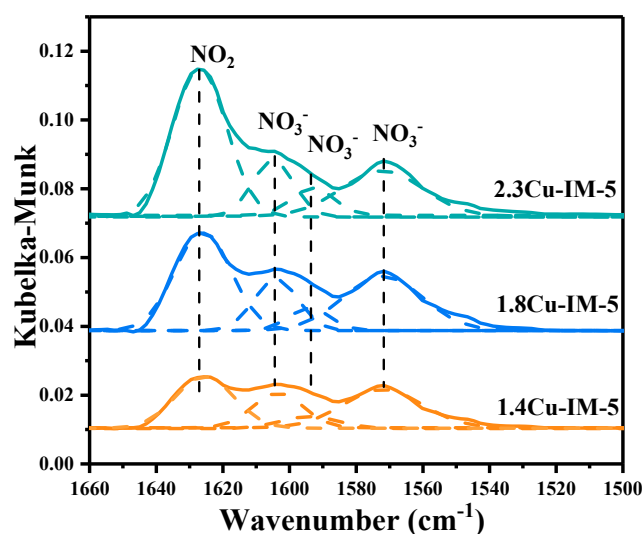


Figure 9. In situ DRIFTS of Cu-IM-5 with different Cu loadings exposed in 500 ppm NO + 5% O<sub>2</sub>.

In situ DRIFTS using NH<sub>3</sub> as a probe molecule is applied to test the acidity of Cu-IM-5. As illustrated in Figure 10, in situ DRIFTS are recorded over 1.4Cu-IM-5 that was exposed to 500 ppm NH<sub>3</sub> flow and purged with N<sub>2</sub> for 30 min. Bands at 3610, 3520, 3338, 3275, 3181, 1625, and 1480 cm<sup>-1</sup> are observed, which are attributed to the adspecies listed in Table 3. In O–H stretch vibration region (3500–3800 cm<sup>-1</sup>), two negative bands located at 3610 cm<sup>-1</sup> and 3520 cm<sup>-1</sup> are assigned to Brønsted acid sites (Zeo–OH groups). They have been consumed by ammonia adsorption over Cu-IM-5 [35,36]. In N–H bending region (1350 cm<sup>-1</sup>–1700 cm<sup>-1</sup>), the band at 1484 cm<sup>-1</sup> is attributed to asymmetric vibration of NH<sub>4</sub><sup>+</sup> adsorbed on Brønsted acid sites ( $\delta(\text{NH}_4^+)$ ), while the band at 1624 cm<sup>-1</sup> is attributed to the N–H bonds of ammonia molecule coordinated with Cu sites [32,37]. In N–H stretching region, the bands at 3338 cm<sup>-1</sup> and 3181 cm<sup>-1</sup> can be assigned to ammonium ions, while the band at 3288 cm<sup>-1</sup> can be assigned to coordinated ammonia molecule [31].

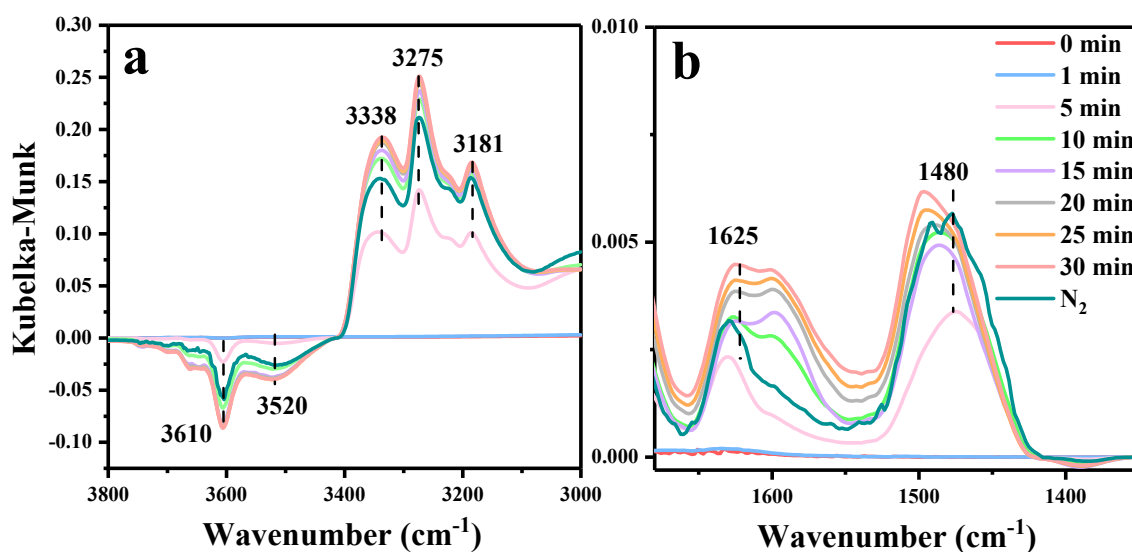
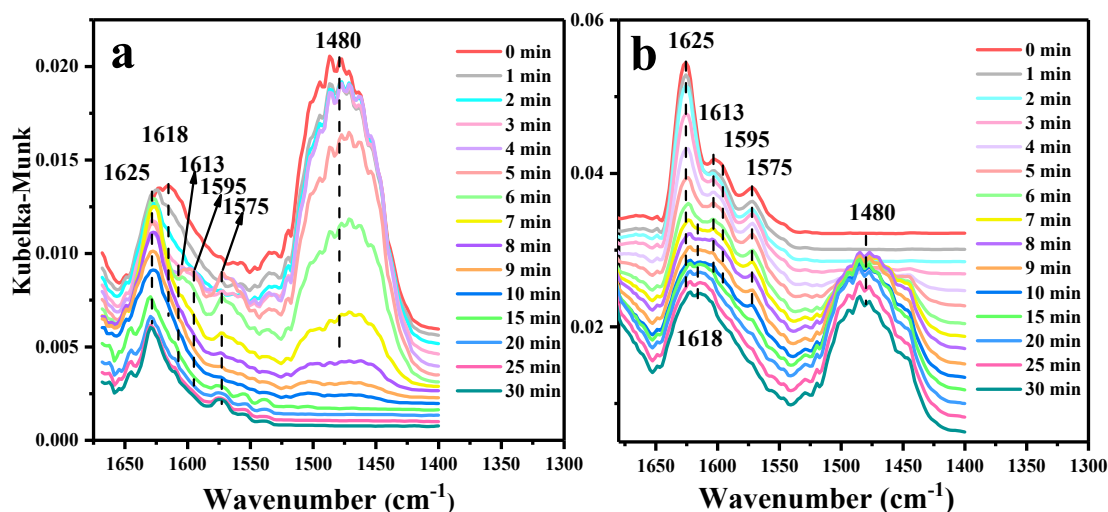


Figure 10. In situ DRIFTS spectra of Cu-IM-5 exposed in (a) 500 ppm NH<sub>3</sub> and (b) purged with N<sub>2</sub>.

In situ DRIFTS study was carried out to follow the reaction between  $\text{NO} + \text{O}_2$  and pre-absorbed  $\text{NH}_3$  in Cu-IM-5, in order to investigate the variation of the adsorbed species on Cu-IM-5 during  $\text{NH}_3$ -SCR reaction. As shown in Figure 11a, the intensity of the band at  $1618 \text{ cm}^{-1}$  declines at the beginning of the reaction. It almost disappears after 5 min, due to the consumption of  $\text{NH}_3$  species on Lewis acid (LA) sites. The band at  $1480 \text{ cm}^{-1}$  decreases slower and disappears until 15 min. The intensity of the band at  $1618 \text{ cm}^{-1}$  decreases faster than that of the band at  $1480 \text{ cm}^{-1}$ .  $\text{NH}_3$  on LA reacts faster with  $\text{NO} + \text{O}_2$  than  $\text{NH}_4^+$  on Brönsted acid (BA) sites. It is generally accepted that Cu ions (LA) are the active sites for SCR, while BA mainly existed as a reservoir of  $\text{NH}_3$  species [32,33,37].  $\text{NH}_4^+$  species on BA migrate to LA to participate  $\text{NH}_3$ -SCR reactions [32].



**Figure 11.** In situ DRIFTS of (a) reaction between 500 ppm  $\text{NO} + 5\% \text{O}_2$  and pre-absorbed  $\text{NH}_3$  on 1.4Cu-IM-5 catalysts and (b) reaction between 500 ppm  $\text{NH}_3$  and pre-absorbed  $\text{NO}_x$  on 1.4Cu-IM-5.

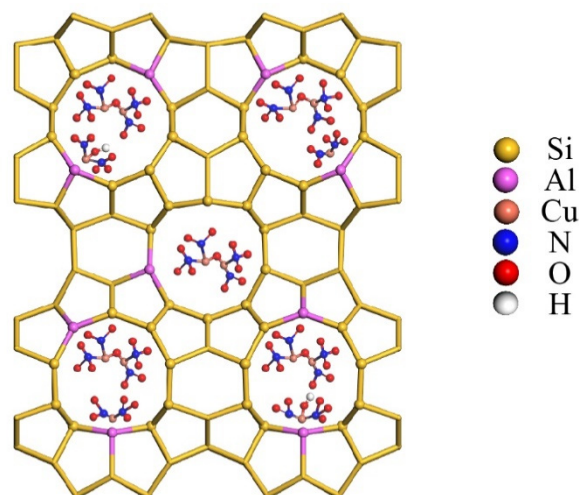
New bands at  $1625, 1613, 1595, 1575,$  and  $1545 \text{ cm}^{-1}$  appear after 5 min, while the peak at  $1480 \text{ cm}^{-1}$  can still be detected. The new bands correspond to formations of nitrates and nitrites.

Figure 11b shows the spectra that were taken on Cu-IM-5 with pre-adsorbed  $\text{NO}_x$  during exposure to  $\text{NH}_3$ . The intensity of bands at  $1625, 1613, 1595, 1575,$  and  $1545 \text{ cm}^{-1}$  reveals the consumption of pre-adsorbed  $\text{NO}_x$  species. The band at  $1480 \text{ cm}^{-1}$  that appears in 5 min suggests a formation of  $\text{NH}_4^+$  on BA. The bands at  $1613, 1595, 1575,$  and  $1545 \text{ cm}^{-1}$  still exist after 5 min.  $\text{NH}_4\text{NO}_3$  may exist as an intermediate during SCR reaction [32]. The bands of  $\text{NO}_2$  and  $\text{NO}_3^-$  disappear completely after 30 min. Ultimately, bands at  $1618 \text{ cm}^{-1}$  and  $1480 \text{ cm}^{-1}$  appear.

### 3. Discussion

Cu contents play a significant role in the  $\text{NH}_3$ -SCR performance of Cu-IM-5.  $\text{NO}_x$  conversion increases slightly with increasing Cu contents at low temperatures ( $<200 \text{ }^\circ\text{C}$ ) and decreases at higher temperatures ( $>200 \text{ }^\circ\text{C}$ ). EPR results suggest the number of isolated Cu ions decreases with increasing Cu contents, while XPS results indicate an increased amount of Cu species on the outer surfaces of Cu-IM-5. A fraction of Cu ions agglomerated during calcination [4]. As indicated by  $\text{H}_2$ -TPR,  $[\text{Cu}(\text{OH})]^+$ , Cu–O–Cu, and  $\text{Cu}^{2+}$  are the main species in Cu-IM-5. Cu–O–Cu species increase with rising Cu contents. Thus, the loss of  $\text{NO}_x$  conversion at higher Cu contents is the consequence of higher amounts of Cu–O–Cu species. Similar to SSZ-13 [38], isolated Cu ions, i.e.,  $[\text{Cu}(\text{OH})]^+$  and  $\text{Cu}^{2+}$ , are the active sites for  $\text{NH}_3$ -SCR in Cu-IM-5. In situ DRIFTS results of  $\text{NO} + \text{O}_2$  adsorption demonstrates that more  $\text{NO}_2$  and  $\text{NO}_3^-$  species form on 2.3Cu-IM-5 (Figure 12). It is reasonable to conclude that  $\text{NO}$  is prone to oxidize on Cu–O–Cu species, which explains

the high performance of 2.3Cu-IM-5 at low temperatures. Higher amounts of Cu–O–Cu species enhance the low-temperature activity of Cu-IM-5 (Table 4). On the contrary, at higher temperatures, NO<sub>x</sub> conversion decreases due to the higher NH<sub>3</sub> oxidation.



**Figure 12.** The framework of Cu-IM-5 and adsorbed NO<sub>x</sub> on different Cu species.

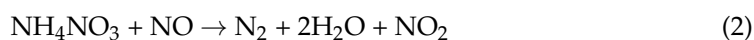
**Table 4.** Adsorbed species over 1.4Cu-IM-5 exposed in NH<sub>3</sub> (Figure 10) or NO+O<sub>2</sub> (Figure 8), and appear (a) and disappear (d) time during reaction (Figure 11).

Wave Number (cm <sup>-1</sup> )	Group	Appear (a) and Disappear (d) Time (min)	
		Figure 11a	Figure 11b
3610	Zeo-OH group	-	-
3275	N-H stretching of NH <sub>4</sub> <sup>+</sup> on BA	-	-
3181 and 3338	N-H stretching of NH <sub>3</sub> on LA	-	-
1618	N-H bending of NH <sub>3</sub> on LA	5 (d)	8 (a)
1480	N-H bending of NH <sub>4</sub> <sup>+</sup> on BA	15 (d)	5 (a)
1625	NO <sub>2</sub>	5 (a)	10 (d)
1615 and 1597	monodentate nitrates	5 (a)	10 (d)
1575	bidentate nitrates	5 (a)	15 (d)

NH<sub>4</sub>NO<sub>3</sub> was observed as an important intermediate during the reactions both between adsorbed NH<sub>3</sub> with NO + O<sub>2</sub> and between adsorbed NO<sub>x</sub> with NH<sub>3</sub>. However, NH<sub>4</sub>NO<sub>2</sub> was not observed, because it has a lower decomposition temperature of 80 °C [22]. NH<sub>4</sub>NO<sub>3</sub> decomposes above 200 °C according to Reaction (1).



In situ DRIFTS was carried out at 150 °C, which is lower than the decomposition temperature. Moreover, N<sub>2</sub> selectivity was very high at this temperature. NH<sub>4</sub>NO<sub>3</sub> is consumed by reacting with NO according to reaction 2 [15].



The freshly formed NO<sub>2</sub> is to be adsorbed again and react further with NH<sub>3</sub>.

## 4. Materials and Methods

### 4.1. Synthesis of Cu-IM-5

As-synthesized IM-5 was provided by SINOPEC Research Institute of Petroleum Processing, Beijing, China. The material was calcined in the air following a temperature

program with a plateau at 290 °C to 550 °C for 4 h. An ion-exchange in 1 L 0.25 M  $\text{CH}_3\text{COONH}_4$  for 5 h at 80 °C was carried out. The obtained  $\text{NH}_4$ -IM-5 was ion-exchanged to Cu-IM-5 in aqueous  $\text{Cu}(\text{NO}_3)_2$  solution with different molarities (1 mM, 3 mM, and 30 mM), and calcined at 550 °C for 4 h. The obtained samples were denoted as 1.4Cu-IM-5, 1.8Cu-IM-5, and 2.3Cu-IM-5, corresponding to 1.4 wt.%, 1.8 wt.%, and 2.3 wt.% Cu contents, respectively.

#### 4.2. Characterization of Cu-IM-5

Powder X-ray diffraction (PXRD) patterns were recorded on a Rigaku SmartLab diffractometer (Tokyo, Japan, Cu  $\text{K}\alpha$  radiation). A Hitachi SU8010 (Tokyo, Japan) scanning electron microscope (SEM) was used to observe crystal morphology and sizes. Elemental compositions were analyzed by ICP-AES on an Optima 8300 (PerkinElmer, Waltham, MA, USA).  $\text{N}_2$ -adsorption isotherms were measured at 77 K with a Micromeritics ASAP 2020 Plus HD88 (Norcross, GA, USA) instrument. The t-plot method was used to calculate the total pore volumes (adsorption branch).

STEM image was carried out on JEM-ARM200P microscope (Tokyo, Japan) with 200 kV acceleration voltage. EDS analysis was performed using a Bruker XFlash 6T160 (Rheinstetten, Germany) apparatus.

$^{29}\text{Si}$  MAS NMR analyses were carried out on Bruker AVANCE III 600 spectrometer at a resonance frequency of 119.2 MHz. The spectra with high-power proton decoupling were recorded with a spinning rate of 10 kHz, a  $\pi/4$  pulse length of 2.6  $\mu\text{s}$ , and a recycle delay of 60 s.  $^{27}\text{Al}$  MAS NMR analyses were carried out at a resonance frequency of 156.4 MHz using a 4 mm HX double-resonance MAS probe at a sample spinning rate of 14 kHz.  $^{27}\text{Al}$  MAS NMR spectra were recorded by a small-flip angle technique with a pulse length of 0.68  $\mu\text{s}$  ( $<\pi/12$ ) and a 1 s recycle delay. The chemical shift of  $^{27}\text{Al}$  was referenced to 1 M aqueous  $\text{Al}(\text{NO}_3)_3$ .

Electron paramagnetic resonance (EPR) experiments were performed on A300-10-12 (Bruker) at the atmosphere.

$\text{H}_2$  temperature-programmed reduction (TPR) was carried out on a homemade chemisorption analyzer equipped with a TCD. A total of 100 mg samples were put into a quartz tube and were pretreated at 350 °C in dry air for 1 h and cooled down to room temperature.  $\text{H}_2$ -TPR was performed in 5%  $\text{H}_2/\text{N}_2$  gas flow of 50 mL/min at a heating rate of 10 °C/min.

For  $\text{NH}_3$ -temperature-programmed desorption ( $\text{NH}_3$ -TPD), the catalyst was purged in  $\text{N}_2$  for 60 min at 350 °C and then exposed in an  $\text{NH}_3/\text{N}_2$  flow for 30 min. Afterward, the catalyst was purged in He flow at 100 °C.  $\text{NH}_3$ -TPD was measured in He of 50 mL/min from 100 to 800 °C with a ramp of 10 °C/min.

In situ DRIFTS experiments were carried out on a Nicolet IS20 spectrometer (Thermo Fisher, Waltham, MA, USA) with an MCT detector and a Harrick high-temperature reaction chamber with ZnSe windows. The sample was purged in 100 mL/min  $\text{N}_2$  flow at 500 °C for 30 min and then cooled down to the reaction temperature. The background spectra were recorded under this temperature. The spectra were measured in the range of 4000–650  $\text{cm}^{-1}$  by accumulating 64 scans at a 4  $\text{cm}^{-1}$  resolution. It is noted that in situ DRIFTS experiments were carried out without the existence of water.

#### 4.3. $\text{NH}_3$ -SCR Test

SCR catalytic performance of Cu-IM-5 was tested on a fixed-bed quartz flow reactor (ID = 4 mm) at atmospheric pressure. 0.1 g catalysts (60–100 mesh) were used. The reaction feed was an  $\text{N}_2$ -based gas mixture containing 500 ppm NO, 500 ppm  $\text{NH}_3$ , and 5%  $\text{O}_2$ . Gas hourly space velocity (GHSV) was fixed at 190,000  $\text{h}^{-1}$ . Reaction temperatures were from 150 °C to 550 °C. The concentrations of  $\text{NO}_x$  were measured using IGS FT-IR (Thermo Fisher) equipped with a 2 m gas cell and an MCT detector with 4  $\text{cm}^{-1}$  resolutions.

$$\text{N}_2 \text{ selectivity}(\%) = \frac{(\text{NO} + \text{NH}_3)_{\text{inlet}} - (\text{NO} + \text{NH}_3)_{\text{outlet}} - (\text{NO}_2 + 2\text{N}_2\text{O})_{\text{outlet}}}{(\text{NO} + \text{NH}_3)_{\text{inlet}} - (\text{NO} + \text{NH}_3)_{\text{outlet}}} \times 100\% \quad (3)$$

$$\text{NO}_x \text{ conversion}(\%) = \frac{(\text{NO})_{\text{inlet}} - (\text{NO} + \text{NO}_2 + 2\text{N}_2\text{O})_{\text{outlet}}}{(\text{NO})_{\text{inlet}}} \times 100\% \quad (4)$$

The kinetic experiments were carried out with 50 mg catalyst (60–100 mesh) and with a volume hourly space velocity of 190,000 h<sup>-1</sup>.

## 5. Conclusions

The Cu-IM-5 catalysts exhibit high NH<sub>3</sub>-SCR performances, which show differences with increasing Cu contents. [Cu(OH)]<sup>+</sup>, Cu–O–Cu and isolated Cu<sup>2+</sup> are the active sites for NH<sub>3</sub>-SCR. The amount of Cu–O–Cu species increases with increasing Cu contents. The low-temperature NH<sub>3</sub>-SCR activity increases with increasing Cu contents due to increasing Cu–O–Cu species. However, the Cu–O–Cu species are more active for NH<sub>3</sub> oxidation at reaction temperatures above 350 °C. In situ DRIFTS suggests an L–H mechanism during NH<sub>3</sub>-SCR over Cu-IM-5 catalysts with NH<sub>4</sub>NO<sub>x</sub> (x = 2 or 3) as the intermediates.

**Author Contributions:** Conceptualization, G.F. and X.Y.; original draft preparation, G.F.; IM-5 preparation, J.C.; characterization, Y.L. and R.L.; writing—review and editing, X.Y. and J.J.; supervision, J.J.; funding acquisition, J.J. All authors have read and agreed to the published version of the manuscript.

**Funding:** This work was funded by the National Natural Science Foundation of China No. 21971259. Weifang Zhengxuan Rare Earth and Catalytic Materials Co., Ltd. is also thanked for financial supports.

**Conflicts of Interest:** The authors declare no conflict of interest.

## References

- Chavannavar, P. Exhaust Aftertreatment System and Method. U.S. Patent No 9,132,386, 3 April 2014.
- Brandenberger, S.; Kröcher, O.; Tissler, A.; Althoff, R. The state of the art in selective catalytic reduction of NO<sub>x</sub> by ammonia using metal-exchanged zeolite catalysts. *Catal. Rev.* **2008**, *50*, 492–531. [[CrossRef](#)]
- Li, R.; Zhu, Y.; Zhang, Z.; Zhang, C.; Fu, G.; Yi, X.; Huang, Q.; Yang, F.; Liang, W.; Zheng, A.; et al. Remarkable performance of selective catalytic reduction of NO<sub>x</sub> by ammonia over copper-exchanged SSZ-52 catalysts. *Appl. Catal. B Environ.* **2021**, *283*, 9641. [[CrossRef](#)]
- Han, L.; Cai, S.; Gao, M.; Hasegawa, J.Y.; Wang, P.; Zhang, J.; Shi, L.; Zhang, D. Selective Catalytic Reduction of NO<sub>x</sub> with NH<sub>3</sub> by Using Novel Catalysts: State of the Art and Future Prospects. *Chem. Rev.* **2019**, *119*, 10916–10976. [[CrossRef](#)]
- Zhang, R.; Liu, N.; Lei, Z.; Chen, B. Selective Transformation of Various Nitrogen-Containing Exhaust Gases toward N<sub>2</sub> over Zeolite Catalysts. *Chem. Rev.* **2016**, *116*, 3658–3721. [[CrossRef](#)]
- Liu, B.; Chen, Z.; Huang, J.; Xia, Q.; Wu, Y.; Chen, H.; Fang, Y. Development of Iron Encapsulated Hollow Beta Zeolites for Ammonia Selective Catalytic Reduction. *Ind. Eng. Chem. Res.* **2019**, *58*, 2914–2923. [[CrossRef](#)]
- Liu, B.; Zheng, K.; Liao, Z.; Chen, P.; Chen, D.; Wu, Y.; Xia, Q.; Xi, H.; Dong, J. Fe-Encapsulated ZSM-5 Zeolite with Nanosheet-Assembled Structure for the Selective Catalytic Reduction of NO<sub>x</sub> with NH<sub>3</sub>. *Ind. Eng. Chem. Res.* **2020**, *59*, 8592–8600. [[CrossRef](#)]
- Liu, B.; Zhao, X.; Mao, W.; Chen, H.; Han, L.; Zhu, K.; Zhou, X. Pickering emulsion mediated crystallization of hierarchical zeolite SSZ-13 with enhanced NH<sub>3</sub> selective catalytic reduction performance. *Micropor. Mesopor. Mater.* **2019**, *285*, 202–214. [[CrossRef](#)]
- Iwamoto, M.; Furukawa, H.; Mine, Y.; Uemura, F.; Mikuriya, S.I.; Kagawa, S.J. Copper(II) ion-exchanged ZSM-5 zeolites as highly active catalysts for direct and continuous decomposition of nitrogen monoxide. *Chem. Soc. Chem. Commun.* **1986**, 1272–1273. [[CrossRef](#)]
- Li, J.; Chang, H.; Ma, L.; Hao, J.; Yang, R.T. Low-temperature selective catalytic reduction of NO<sub>x</sub> with NH<sub>3</sub> over metal oxide and zeolite catalysts—A review. *Catal. Today* **2011**, *175*, 147–156. [[CrossRef](#)]
- Baerlocher, C.; Gramm, F.; Massüger, L.; McCusker, L.B.; He, Z.; Hovmöller, S.; Zou, X. Structure of the Polycrystalline Zeolite Catalyst IM-5 Solved by Enhanced Charge Flipping. *Science* **2007**, *315*, 1113–1116. [[CrossRef](#)] [[PubMed](#)]
- Tu, C.; Chen, J.; Li, W.; Wang, H.; Deng, K.; Vinokurov, V.A.; Huang, W. Hydrodeoxygenation of bio-derived anisole to cyclohexane over bi-functional IM-5 zeolite supported Ni catalysts. *Sustain. Energy Fuels* **2019**, *3*, 3462–3472. [[CrossRef](#)]
- Zhang, J.; Tian, F.; Chen, J.; Shi, Y.; Cao, H.; Ning, P.; Sun, S.; Xie, Y. Conversion of phenol to cyclohexane in the aqueous phase over Ni/zeolite bi-functional catalysts. *Front. Chem. Sci. Eng.* **2020**. [[CrossRef](#)]
- Vennestrøm, P.N.R.; Janssens, T.V.W.; Kustov, A.; Grill, M.; Molina, P.A.; Lundegaard, L.F.; Tiruvalam, R.R.; Concepción, P.; Corma, A.J. Influence of lattice stability on hydrothermal deactivation of Cu-ZSM-5 and Cu-IM-5 zeolites for selective catalytic reduction of NO<sub>x</sub> by NH<sub>3</sub>. *J. Catal.* **2014**, *309*, 477–490. [[CrossRef](#)]

15. Moretti, G.; Ferraris, G.; Fierro, G.; Jacono, M.L.; Morpurgo, S.; Faticanti, M.J. Dimeric Cu(I) species in Cu-ZSM-5 catalysts: The active sites for the NO decomposition. *J. Catal.* **2005**, *232*, 476–487. [[CrossRef](#)]
16. Centi, G.; Perathoner, S. Nature of active species in copper-based catalysts and their chemistry of transformation of nitrogen oxides. *Appl. Catal. Gen* **1995**, *132*, 179–259. [[CrossRef](#)]
17. Dzwigaj, S.; Janas, J.; Gurgul, J.; Socha, R.P.; Shishido, T.; Che, M. Do Cu(II) ions need Al atoms in their environment to make CuSiBEA active in the SCR of NO by ethanol or propane? A spectroscopy and catalysis study. *Appl. Catal. B Environ.* **2009**, *85*, 131–138. [[CrossRef](#)]
18. Gao, F.; Peden, C.H.F. Recent Progress in Atomic-Level Understanding of Cu/SSZ-13 Selective Catalytic Reduction Catalysts. *Catalysts* **2018**, *8*, 140. [[CrossRef](#)]
19. Gao, F.; Walter, E.D.; Washton, N.M.; Szanyi, J.; Peden, C.H.F. Synthesis and Evaluation of Cu-SAPO-34 Catalysts for Ammonia Selective Catalytic Reduction. 1. Aqueous Solution Ion Exchange. *ACS Catal.* **2013**, *3*, 2083–2093. [[CrossRef](#)]
20. Liu, L.L.; Liu, L.; Cao, Y.; Wang, J.; Si, R.; Gao, F.; Dong, L. Controlling Dynamic Structural Transformation of Atomically Dispersed CuO<sub>x</sub> Species and Influence on Their Catalytic Performances. *ACS Catal.* **2019**, *9*, 9840–9851. [[CrossRef](#)]
21. Kwak, J.H.; Lee, J.H.; Burton, S.D.; Lipton, A.S.; Peden, C.H.F.; Szanyi, J. A Common Intermediate for N<sub>2</sub> Formation in Enzymes and Zeolites: Side-On Cu–Nitrosyl Complexes. *Angew. Chem. Int. Ed.* **2013**, *52*, 9985–9989. [[CrossRef](#)] [[PubMed](#)]
22. Szanyi, J.; Kwak, J.H.; Zhu, H.; Peden, C.H.F. Characterization of Cu-SSZ-13 NH<sub>3</sub> SCR catalysts: An in situ FTIR study. *Phys. Chem. Chem. Phys.* **2013**, *15*, 2368–2380. [[CrossRef](#)] [[PubMed](#)]
23. Long, R.Q.; Yang, R.T. Reaction Mechanism of Selective Catalytic Reduction of NO with NH<sub>3</sub> over Fe-ZSM-5 Catalyst. *J. Catal.* **2002**, *207*, 224–231. [[CrossRef](#)]
24. Iwasaki, M.; Yamazaki, K.; Banno, K.; Shinjoh, H.J. Characterization of Fe/ZSM-5 DeNO<sub>x</sub> catalysts prepared by different methods: Relationships between active Fe sites and NH<sub>3</sub>-SCR performance. *J. Catal.* **2008**, *260*, 205–216. [[CrossRef](#)]
25. Yu, T.; Hao, T.; Fan, D.; Wang, J.; Shen, M.; Li, W.J. Recent NH<sub>3</sub>-SCR Mechanism Research over Cu/SAPO-34 Catalyst. *Phys. Chem. C* **2014**, *118*, 6565–6575. [[CrossRef](#)]
26. Chen, B.; Xu, R.; Zhang, R.; Liu, N. Economical way to synthesize SSZ-13 with abundant ion-exchanged Cu<sup>+</sup> for an extraordinary performance in selective catalytic reduction (SCR) of NO<sub>x</sub> by ammonia. *Environ. Sci. Technol.* **2014**, *48*, 13909–13916. [[CrossRef](#)] [[PubMed](#)]
27. Nanba, T.; Masukawa, S.; Ogata, A.; Uchisawa, J.; Obuchi, A. Active sites of Cu-ZSM-5 for the decomposition of acrylonitrile. *Appl. Catal. B Environ.* **2005**, *61*, 288–296. [[CrossRef](#)]
28. Occhiuzzi, M.; Fierro, G.; Ferraris, G.; Moretti, G. Unusual Complete Reduction of Cu<sup>2+</sup> Species in Cu-ZSM-5 Zeolites under Vacuum Treatment at High Temperature. *Chem. Mater.* **2012**, *24*, 2022–2031. [[CrossRef](#)]
29. Peng, C.; Yan, R.; Peng, H.; Mi, Y.; Liang, J.; Liu, W.; Wang, X.; Song, G.; Wu, P.; Liu, F.J. One-pot synthesis of layered mesoporous ZSM-5 plus Cu ion-exchange: Enhanced NH<sub>3</sub>-SCR performance on Cu-ZSM-5 with hierarchical pore structures. *Hazard. Mater.* **2020**, *385*, 1593. [[CrossRef](#)]
30. Shan, Y.; Du, J.; Yu, Y.; Shan, W.; Shi, X.; He, H. Precise control of post-treatment significantly increases hydrothermal stability of in-situ synthesized Cu-zeolites for NH<sub>3</sub>-SCR reaction. *Appl. Catal. B Environ.* **2020**, *266*, 8655. [[CrossRef](#)]
31. Gao, F.; Wang, Y.; Washton, N.M.; Kollár, M.; Szanyi, J.; Peden, C.H.F. Effects of Alkali and Alkaline Earth Cations on the Activity and Hydrothermal Stability of Cu/SSZ-13 NH<sub>3</sub>-SCR Catalysts. *ACS Catal.* **2015**, *5*, 6780–6791. [[CrossRef](#)]
32. Wang, D.; Zhang, L.; Kamasamudram, K.; Epling, W.S. In Situ-DRIFTS Study of Selective Catalytic Reduction of NO<sub>x</sub> by NH<sub>3</sub> over Cu-Exchanged SAPO-34. *ACS Catal.* **2013**, *3*, 871–881. [[CrossRef](#)]
33. Ma, L.; Cheng, Y.; Cavataio, G.; McCabe, R.W.; Fu, L.; Li, J. In situ DRIFTS and temperature-programmed technology study on NH<sub>3</sub>-SCR of NO<sub>x</sub> over Cu-SSZ-13 and Cu-SAPO-34 catalysts. *Appl. Catal. B Environ.* **2014**, *156–157*, 428–437. [[CrossRef](#)]
34. Olsson, L.; Sjövall, H.; Blint, R.J. Detailed kinetic modeling of NO<sub>x</sub> adsorption and NO oxidation over Cu-ZSM-5. *Appl. Catal. B Environ.* **2009**, *87*, 200–210. [[CrossRef](#)]
35. Zhu, H.; Kwak, J.H.; Peden, C.; Szanyi, J. In situ DRIFTS-MS studies on the oxidation of adsorbed NH<sub>3</sub> by NO<sub>x</sub> over a Cu-SSZ-13 zeolite. *Catal. Today* **2013**, *205*, 16–23. [[CrossRef](#)]
36. Zhang, T.; Shi, J.; Liu, J.; Wang, D.; Zhao, Z.; Cheng, K.; Li, J. Enhanced hydrothermal stability of Cu-ZSM-5 catalyst via surface modification in the selective catalytic reduction of NO with NH<sub>3</sub>. *Appl. Surf. Sci.* **2016**, *375*, 186–195. [[CrossRef](#)]
37. Sjövall, H.; Fridell, E.; Blint, R.J.; Olsson, L. Identification of adsorbed species on Cu-ZSM-5 under NH<sub>3</sub> SCR conditions. *Top. Catal.* **2007**, *42*, 113–117. [[CrossRef](#)]
38. Song, J.; Wang, Y.; Walter, E.D.; Washton, N.M.; Mei, D.; Kovarik, L.; Engelhard, M.H.; Proding, S.; Wang, Y.; Peden, C.H.F.; et al. Toward Rational Design of Cu/SSZ-13 Selective Catalytic Reduction Catalysts: Implications from Atomic-Level Understanding of Hydrothermal Stability. *ACS Catal.* **2017**, *7*, 8214–8227. [[CrossRef](#)]